Electronic Supplementary Material (ESI) for Materials Horizons.

Supporting Information

Nanofocusing of circularly polarized Bessel-type plasmon polaritons with hyperbolic metamaterials

*Ling Liu, Ping Gao, Kaipeng Liu, Weijie Kong, Zeyu Zhao, Mingbo Pu, Changtao Wang and Xiangang Luo**

State Key Laboratory of Optical Technologies on Nano-Fabrication and Micro-Engineering, Institute of Optics and Electronics, Chinese Academy of Science, P.O. Box 350, Chengdu 610209, China.

**Email address: lxg@ioe.ac.cn*

1□ The optical property of adhesive material

As described in Fig. S1(a), the transmitted spectrum measured by ellipsometer (SE 850, SENTECH) shows that the transmittance of the adhesive layer has reached to 91% at 365 nm wavelength. Figure S1(b) exhibits that the real part permittivity of adhesive material is 2.33 at the 365 nm working wavelength. From Fig. S1(c), it could be seen that the transmitted intensity of the main lobe decreases with the adhesive layer thickness ranging from 0 nm to 70 nm. This phenomenon is mainly attributed to weakened resonance effect of the guided mode resonance structure composed by mask and adhesive layer as the adhesive layer thickness increases, which delivers low transmitted intensity of the main lobe. At the same time, Fig. S1(d) shows that when the adhesive layer thickness changes from 0 nm to 30 nm, the normalized transmitted intensity profiles in the middle of the Pr region overlap each other and the FWHM of the transverse profiles remain 62 nm.

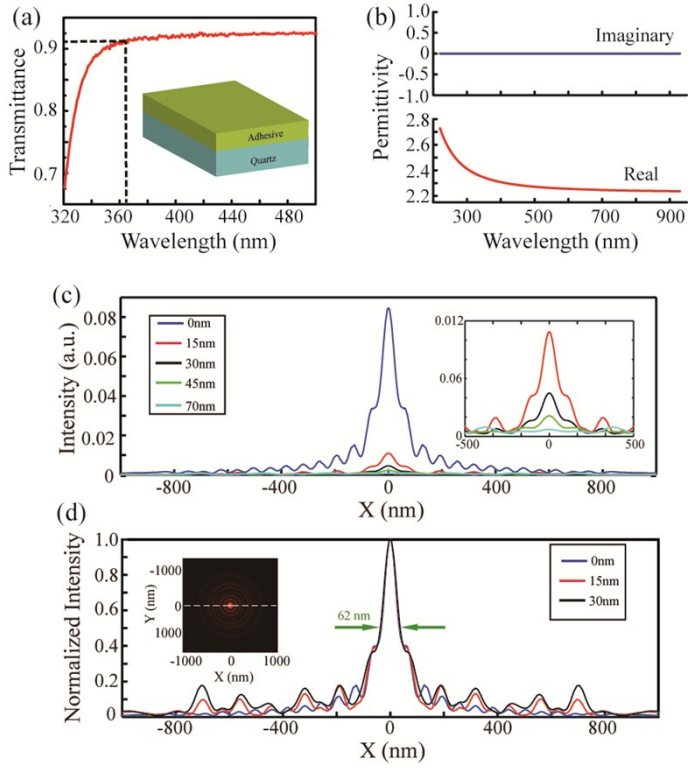

Fig. S1. (a) The transmission spectrum of the adhesive material. (b) The measured permittivity of adhesive layer. (c) The intensity and (d) Normalized intensity distributions in the middle of the Pr region along the white dashed line in inset of (d) for different adhesive material thickness. The other simulated parameters are the same as those in Fig. 1.

2□ The effect of the diameter of the innermost ring, and the thickness of metal and dielectric film on focusing spot

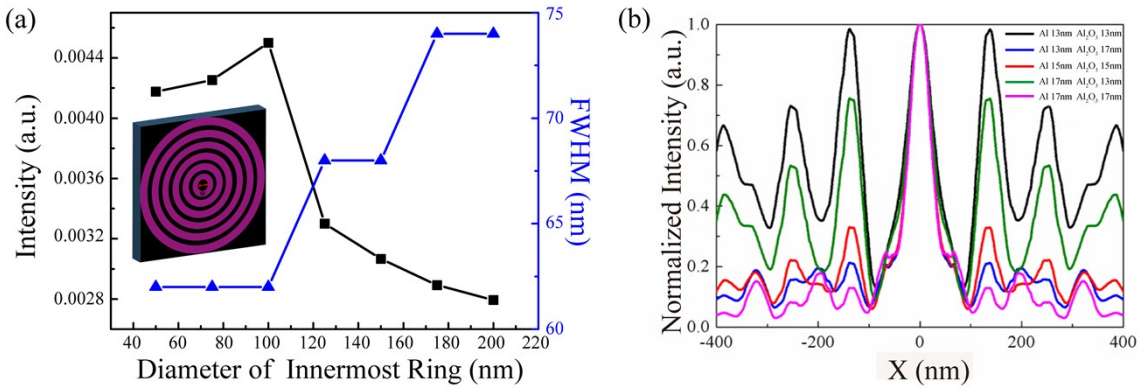

Fig. S2. (a) The variation of intensity and FWHM of the focusing spot by changing the diameter of innermost ring (W). (b) Dependence of normalized intensity on different thickness of Al and Al_2O_3 film. The other parameters are the same as those in Fig. 1.

As depicted in Fig. S2(a), the intensity changes slightly when the diameter of innermost ring varies from 50nm to 100nm. At the same time, the FWHM of focus spot maintains 62nm throughout. However, the intensity rapidly decreases and FWHM of the hot spot enlarges to 74nm as the diameter increases beyond 100nm. So, the diameter of innermost ring could be chosen as 100nm considering the intensity and the size of spot simultaneously.

From Fig. S2(b), one can see that the influence of thickness of dielectric layer on normalized intensity is more obvious than that of the thickness of metal layer, which is attributed to the concentration of electric fields in the dielectric layer caused by the resonance effect of BPP waves. Furthermore, when the thickness of dielectric layer Al_2O_3 is lower than 15nm, the normalized intensity of side lobe could not be efficiently suppressed. Considering the transmittance of the multilayer structure in experiment, the 15-nm-thick for single metal and dielectric film could be chosen in simulation. On the other hand, Fig. S2(b) also shows that in fabrication process, +2nm error for dielectric thickness and ±2nm error for metal thickness could be accepted, respectively.

3、Determination for the metal material and periods of multilayer structure.

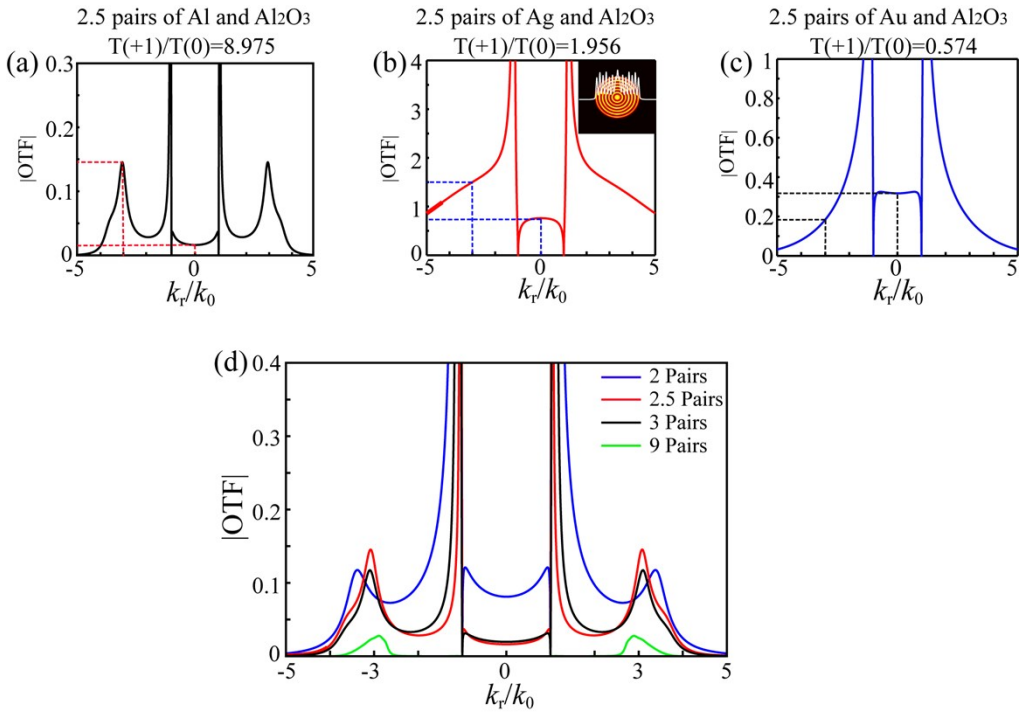

Fig. S3. Optical transfer function in the measure of $|H_y|$ for the HMM composed by (a) Aluminum and Alumina. (b) Silver and Alumina. (c) Gold and Alumina. (d) Aluminum and Alumina with different pairs.

As exhibited in the Fig. S3(a), the transmitted window of the HMM composed of alternative aluminum and alumina multilayer has a narrow band around $k_r=3k_0$, resulting that the BPP wave with the wavevector $3k_0$ could be coupled out the metamaterial and other diffraction waves outside the window range are damped. As shown in Fig. S3(b) and (c), if the Ag or Au is chosen as the metal layer instead of Al, the narrow filtering window disappears, which results in a damped transmitted amplitude ratio of the HMM for +1 order and 0 order diffracted wave, i.e. $T(+1)/T(0)$. Therefore, the low transmitted ratio leads to the strong interference effect between 0 order and +1 order diffracted wave and no focusing spot could be found in simulation as shown in inset of Fig. S3(b). That is because the real parts of the permittivity of Ag and Au are close to the permittivity of alumina (ε_{Al2O3}=3.218). The permittivities for the aluminum, silver and gold at λ=365 nm in simulation are ε_{Al}=-19.46+3.6i, ε_{Ag}=-2.4+0.24i and ε_{Au}=-2.4710+3.0144i, respectively.

The periods of the metal- Al_2O_3 unit cell structure are also determined by the transmitted amplitude ratio for +1 order and 0 order diffracted wave. Figure S3(d) clearly shows that a

filtering window with low absorption for the specific BPP waves around the wavevector $3k_0$ is created through 2 pairs and a half, and 3 pairs Al/Al_2O_3 multilayer metamaterial. But under 2 pairs of multilayer metamaterial, the transmitted amplitude of 0 order diffracted wave is not efficiently suppressed. At the same time, as shown in Fig. S3(d), the other diffraction waves could be better suppressed with more pairs of the Al and Al_2O_3, only filtering the +1 order diffracted wave ($3k_0$), but the transmitted amplitude decrease more quickly than that through the multilayer metamaterial with 2 pairs and a half. Considering the trade-off between the number of multilayer metamaterial and the transmission efficiency, the 2 pairs and a half of multilayer could be chosen, although the filtering window for low frequency is not the absolutely closed.

4、The effect of dimension of the plasmonic cavity lens on its optical properties

Figure S4(a) is the schematic configuration of plasmonic cavity lens. Figure S4(b) shows that the transmission amplitude ratio of E_r and E_z maintains constant versus the changed radial wavevectors with different Ag thickness d_1. But the maximal value of amplitudes of E_r and E_z are simultaneously achieved at the thickness of top Ag d_1=20 nm, not d_1=0 nm, when the radial wavevector is fixed $3k_0$ shown in Fig. S4(c). So the thickness d_1 of top Ag for 20 nm has been chosen. Figure S4(d) exhibits that high permittivity of dielectric layer delivers improvement of the magnitude ratio of the electric field components E_r and E_z at the radial wavevector of k_r=$3k_0$. The permittivity of the commercial photoresist used in experiment as the dielectric layer in the Ag/dielectric/Ag cavity structure is 2.59. As illustrated in inset of Fig. S4(e), when the dielectric layer thickness is 30 nm, the magnitude ratio of the electric field components E_r and E_z could be reached maximal value of about 3.62. From the inset of Fig. S4(f), it could be seen that transmission amplitude ratio of the E_r and E_z changes slightly when the bottom Ag thickness d_3 is higher than 70 nm, and the thickness of bottom Ag film as a plasmonic reflector must be larger than the skin depth of Ag. So we choose the thickness of bottom Ag for 70 nm. Compared with the effect of the top Ag film on adjusting the magnitude ratio of the electric field components E_r and E_z, Fig. S4(f) also indicates that the

reflection effect of the Ag layer deposited beneath a Pr layer dominates in the enhancement of the magnitude ratio of the electric field components E_r and E_z at the radial wavevector of $k_r=3k_0$.

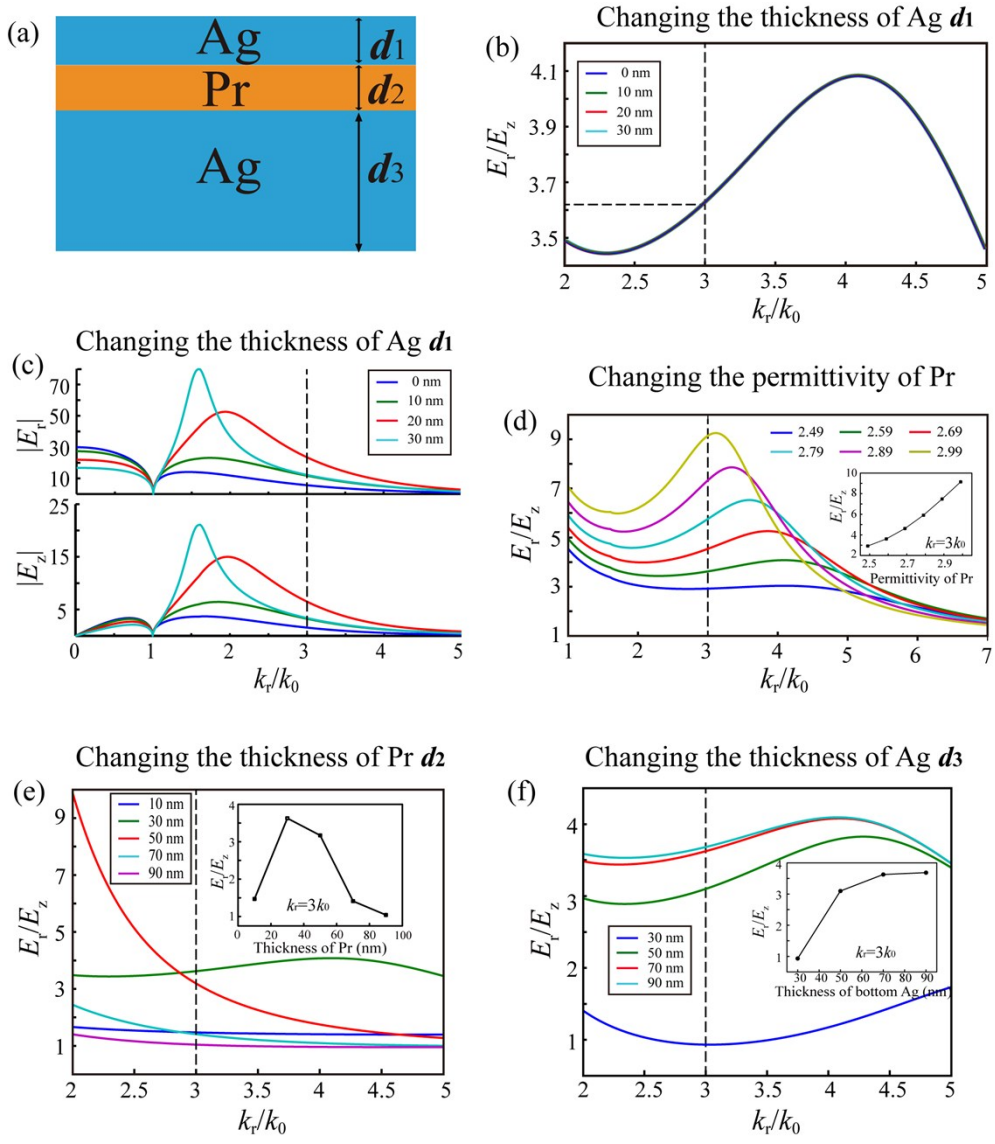

Fig. S4. (a)The schematic of plasmonic cavity lens. (b)The transmission amplitude ratio of the electric field components E_r and E_z versus different radial wavevectors with different thickness d_1 of top Ag. (c) The transmission amplitudes of E_r and E_z with different radial wavevector by applying variant thickness d_1 of top Ag. The magnitude ratio of the electric field components E_r and E_z distributions with different radial wavevectors by changing the (d) The permittivity of Pr. (e) The thickness d_2 of Pr. (f) The thickness d_3 of bottom Ag.

5、The optical transfer function of Pr layer and plasmonic cavity lens

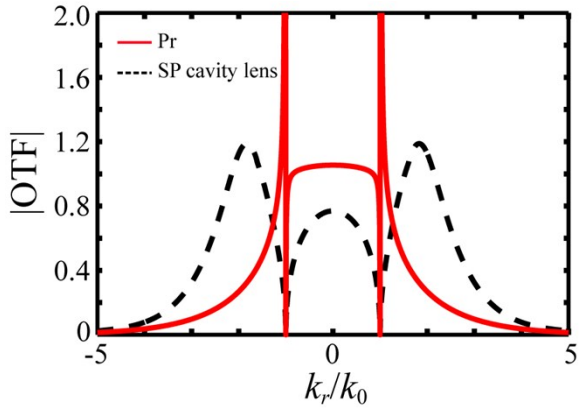

Fig. S5. The optical transfer function in the measure of $|H_y|$ of the Bessel-BPPs focusing structure with Pr and plasmonic cavity lens.

6、Exposure dose discussion based on size of focusing spot

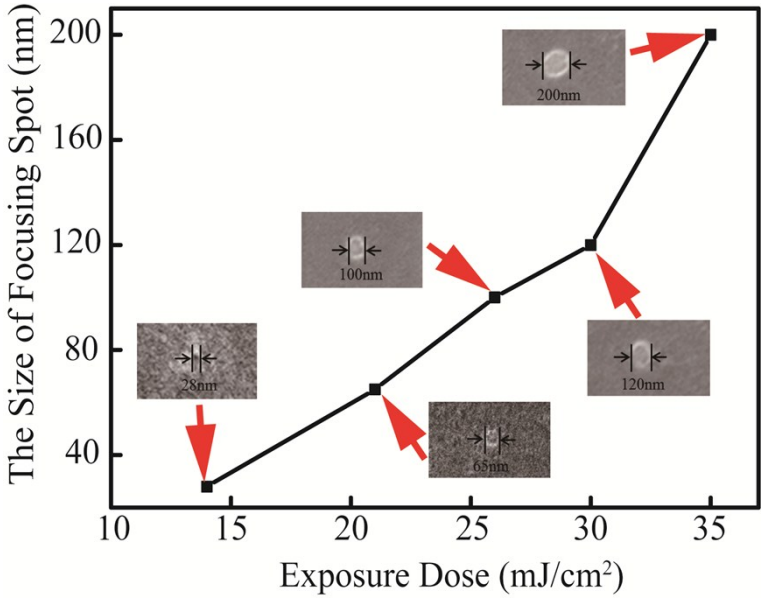

Fig. S6. The size of spot versus exposure dose at a fix working distance of 40 nm.

As an example, we studied the spot size as a function of exposure dose at 40nm working distance. Figure S6 shows that exposure dose plays a significant role in determining the spot size. With the same developer, the spot size increases with the exposure dose. From the SEM inspection, the first spot was visible at a dose of 14 mJ/cm^2, although the size of spot could be shrunken to 28nm, but there was consistency in the obtained spot since for near threshold exposure, so any variations can cause a large change in the results. Below this dose, the spot

was not visible at all. When the exposure dose was increased to 22 mJ/cm^2, the edge of the focusing spot became clear, and the measured size of spot was ~65 nm, which is in agreement with the theoretical analysis result. However, further increase of the dose would lead to overexposure because the spots were larger than the outline dimension of simulation. To find the optimum exposure time, we design the concentric annular grating patterns with the same dimensions in 5 different regions on the same mask. In experiments, the five patterns are illuminated under different exposure doses by adjusting different exposure times. Through the experiments, 22 mJ/cm^2 was identified as the optimal exposure dose. Although there is difference of the optimum experiment dose among repeatable experiments due to the errors in fabrication processes, these differences are acceptable. Besides, the illuminated power densities used to calculate the exposure dose refer to the transmitted energy penetrating Bessel beam generating structure and corresponding space layer instead of directly taken from UV source.

7、The fabrication flow of sample and the process of lithography

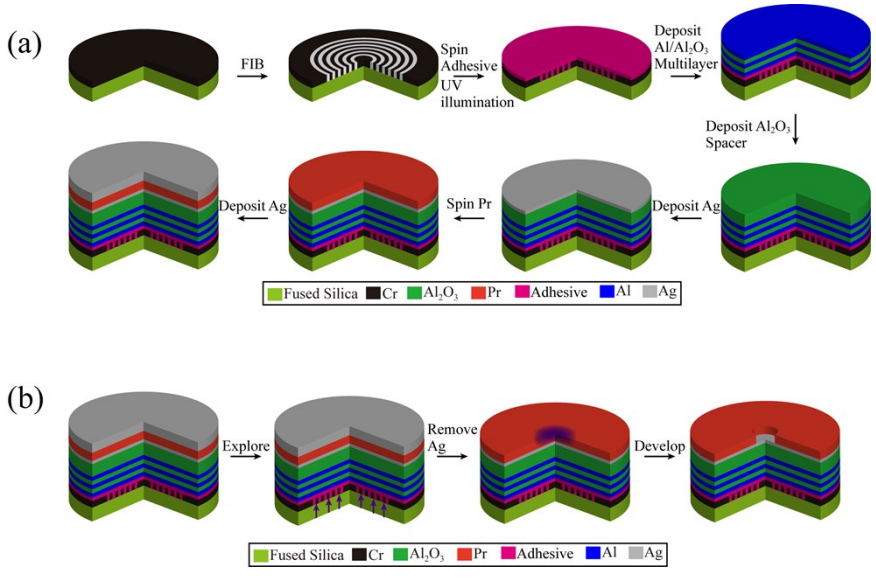

Fig. S7. (a) Fabrication flow of the sample. (b) The lithography process.

8、The effect of divergent angle of the incident light on focusing spot

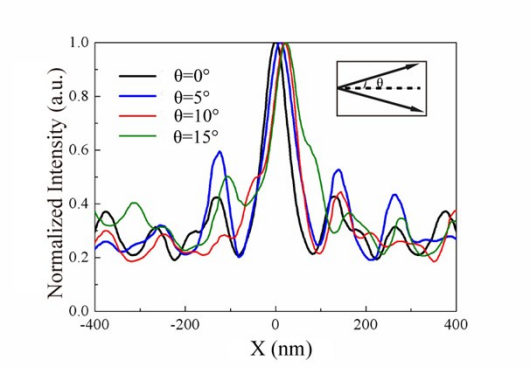

Fig. S8. The normalized intensity distribution for different divergent angle θ of the incident light.

The light source with 365 nm wavelength used in the experiment is provided by LED OEM module (LASERPRODUKTE GMBH, GERMANY), which could be connected to the machine or programmable logic controller. The measured divergent angle θ of the incident light is 14° in experiment. Figure S8 shows that when the divergent angle θ reaches above 10°, the center peaks of the normalized intensity become asymmetrical which remarkably enlarge the size of the focusing spot. In order to eliminate the effect of the divergent angle on focusing spot, an ultraviolet biconvex lens with 12mm diameter and 12mm (NA=0.45, θ=26.5°) focal length is positioned in front of a linear polarizer (P) and a quarter wave plate (QWP) to generate the desired circularly polarized light illumination.